Submitted to the
XXI International Symposium on Lepton and Photon Interactions at High Energies
11-16 August 2003 Fermi National Accelerator Laboratory, Batavia, Illinois USA

Abstract:

Measurement of the electromagnetic component of photon light-cone wave function at HERA

ZEUS Collaboration

Abstract

The lowest component of the real photon electromagnetic light-cone wave function was measured with the ZEUS detector at HERA through an exclusive production of dimuons, $ep \to e\mu^+\mu^-p$, the diffractive dissociation of a real photon to a dimuon system. The measurement was carried out using the data collected during 1999-00 with an integrated luminosity of 55.4 pb^{-1}. The events were selected for γp centre-of-mass energies $30 < W < 170\,\mathrm{GeV}$, mass of dimuon system $4 < M_{\mu\mu} < 15\,\mathrm{GeV}$, square of the four momentum exchanged at the proton vertex $|t| < 0.5\,(\mathrm{GeV/c})^2$ and transverse momentum of the muon with respect to the real photon $k_T > 1.2\,\mathrm{GeV/c}$. Differential cross section presented as function of u, the fraction of longitudinal light-cone momentum carried by the muon, shows agreement with the theoretical predictions, providing the first proof that diffractive dissociation of particles can be reliably used to measure their light-cone wave function.

1 Introduction

1.1 Light-Cone Wave Functions

The internal structure of hadrons and photons is described through the light-cone wave functions (LCWF). These functions are constructed from the QCD light-cone Hamiltonian: $H_{LC}^{QCD} = P^+P^- - P_\perp^2$ where $P^\pm = P^0 \pm P^z$ with P the momentum operators [1]. The LCWF ψ_h for a hadron h with mass M_h satisfies the relation: $H_{LC}^{QCD}|\psi_h\rangle = M_h^2|\psi_h\rangle$. Measurement of the LCWF can therefore test the interaction described by the Hamiltonian. The LCWF are expanded in terms of a complete basis of Fock states having increasing complexity [1]. For example, the negative pion has the Fock expansion:

$$\begin{aligned} |\psi_{\pi^-}> &= \sum_n <n|\pi^-> |n> \\ &= \psi^{(\Lambda)}_{d\bar{u}/\pi}(u_i, \vec{k}_{\perp i})|\bar{u}d> \\ &\quad +\psi^{(\Lambda)}_{d\bar{u}g/\pi}(u_i, \vec{k}_{\perp i})|\bar{u}dg> + \cdots \end{aligned} \tag{1}$$

They have longitudinal light-cone momentum fractions:

$$u_i = \frac{k_i^+}{p^+} = \frac{k_i^0 + k_i^z}{p^0 + p^z}, \qquad \sum_{i=1}^n u_i = 1 \tag{2}$$

and relative transverse momenta

$$\vec{k}_{\perp i} \quad , \qquad \sum_{i=1}^n \vec{k}_{\perp i} = \vec{0}_\perp. \tag{3}$$

where the index i runs over the particles contained in the relevant Fock state, e.g. n=2 for $\psi_{d\bar{u}}$, n=3 for $\psi_{d\bar{u}g}$.
The first term in the expansion is referred to as the valence Fock state, as it relates to the hadronic description in the constituent quark model.

1.2 The Photon LCWF

The photon LCWF can be described similar to that of the pion except that it has two major components: the electromagnetic and the hadronic states:

$$\begin{aligned} \psi_\gamma = a|\gamma_p\rangle + b|l^+l^-\rangle + c|l^+l^-\gamma\rangle + (other\ e.m.) \\ +d|q\bar{q}\rangle + e|q\bar{q}g\rangle + (other\ hadronic) + ...\ , \end{aligned} \tag{4}$$

where $|\gamma_p\rangle$ describes the point bare-photon and $|l^+l^-\rangle$ stands for $|e^+e^-\rangle$, $|\mu^+\mu^-\rangle$ etc. Each of these states is a sum over the relevant helicity components. The wave function of the photon is very rich: it can be studied for real photons, for virtual photons of various virtualities, for transverse and longitudinal photons. The LCWF for the lowest Fock states is given by [2]:

$$\psi^{\lambda}_{\lambda_1\lambda_2}(k_\perp, u) = \; - \, ee_f \, \frac{\overline{f}_{\lambda_1}(k)\lambda \cdot \epsilon^{\lambda} f_{\lambda_2}(q-k)}{\sqrt{u(1-u)}\left(Q^2 + \frac{k_\perp^2 + m^2}{u(1-u)}\right)} \tag{5}$$

where ϵ^λ is the polarization vector and $f_\lambda, m,\ \lambda_1,\ \lambda_2,\ ee_f$ are the fermion distributions, masses, helicities and charges, respectively. Q^2 is the photon virtuality. The wave function of this component for $k_\perp^2 \gg \Lambda^2_{QCD}$ is expected to be similar for the electromagnetic and hadronic components. The probability amplitude Φ^2 is obtained from the trace of this function. For transversly polarized photon the result is:

$$\Phi^2_{f\bar{f}/\gamma^*_T} \sim \sum_{\mu=1}^{2} \frac{1}{4} Tr\psi^2 = \frac{m^2 + k_\perp^2[u^2 + (1-u)^2]}{[k_\perp^2 + a^2]^2} \tag{6}$$

where $a^2 = m^2 + Q^2 u(1-u)$.

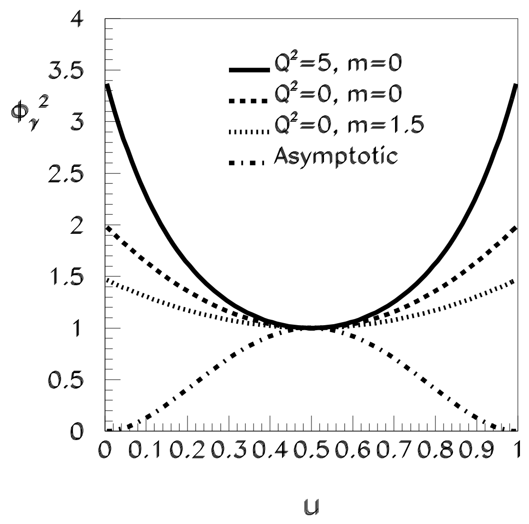

Figure 1: *The photon wave function for transverse virtual photons (Q^2 = 5 (GeV/c)^2) and massless quarks/leptons (solid line), real photons and massless quarks/leptons (dashed line), real photons and charm quarks (dotted line) and the asymptotic function (dashed-dotted line). The functions are arbitrarily normalized at $u = 0.5$.*

The predicted LCWF for the electromagnetic component are based on quantum electrodynamics and can be considered precise. Those for the hadronic component are model dependent. Examples of Φ^2 calculated using Eq. 1 and the asymptotic LCWF suggested for the hadronic component [3] are shown in Fig. 1.

1.3 Measurement of the LCWF in diffractive dissociation

Most measurements of the LCWF have been done by measuring form factors, but have proved to be rather insensitive to the structure of the LCWF [4]. Recent measurements of the pion LCWF in diffractive dissociation [5] have show that this method is sensitive to the LCWF structure.

The concept of these measurements and of the present work is the following: a high energy particle dissociates diffractively through some interaction. The first (valence) Fock component dominates while the other terms are suppressed according to counting rules [4] [6]. In this process the quarks break apart and hadronize into two jets. Measurement of the jet momenta gives the quark momenta.

In this paper a measurement of the electromagnetic component of the real photon LCWF is presented. This was done using the exclusive $ep \to e\mu^+\mu^- p$ photoproduction process.

2 Data analysis

The data used in this analysis were collected at HERA ep collider during 1999-2000 with ZEUS [7] detector. At that time HERA operated at proton energy of 920 GeV and at positron energy of 27.5 GeV. The integrated luminosity used was 55.4 ± 1.3 pb^{-1}. The events of the exclusive reaction were triggered using the muon chambers [8]. At the offline level each event was demanded to have two high quality tracks from the central tracking detector (CTD) [9], fitted to the vertex and matched to energy deposits in the uranium calorimeter (CAL) [10]. No signal from the scattered positron was required in the CAL. To select exclusive events, a requirement was imposed that the energy deposited in the forward proton calorimeter (FPC) [11] was belowed 1 GeV. The FPC is a detector able to identify particles emitted at low polar angle along the proton direction, in our case coming from the proton dissociation. The following kinematic variables (see Fig. 2), reconstructed from the momenta of the CTD tracks, were used to define the phase space region of the measurement:

$$u = \frac{E_1 + p_{z1}}{E_1 + p_{z1} + E_2 + p_{z2}} \tag{7}$$

$$W^2 = (q+P)^2 \sim 2E_p \sum_i (E_i + p_{zi}) \tag{8}$$

$$
\begin{aligned}
t &= (P-P')^2 \sim p_T^2(\mu\mu) && (9)\\
M_{\mu\mu}^2 &= (p_1+p_2)^2 && (10)\\
\vec{k}_{T1}+\vec{k}_{T2} &= \vec{0} && (11)
\end{aligned}
$$

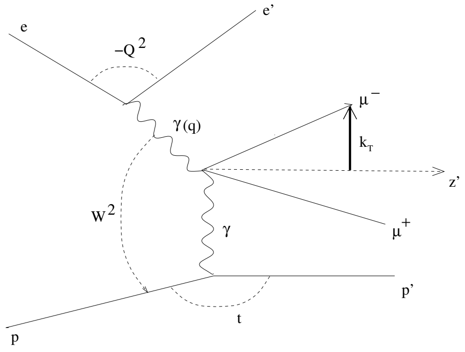

Figure 2: *Definition of the kinematic variables.*

where u is the longitudinal momentum-fraction carried by the muon, W the γp centre of mass energy, t the square of the four momentum exchanged at the proton vertex, $M_{\mu\mu}$ the invariant mass of the dimuon system and k_T the transverse momentum of a muon with rescpect to the real photon. In Eqs. 7-11 E_1, p_1, E_2, p_2 are the energy and momentum of each muon.

The kinematic region was defined by the following selection criteria: $4 < M_{\mu\mu} < 15\,\mathrm{GeV}$, $30 < W < 170\,\mathrm{GeV}$ (in order to remain in a region of stable and high acceptance), $|t| < 0.5\,\mathrm{GeV}^2$ (to select exclusive events), $0.1 < u < 0.9$ (to avoid region of low acceptance), $k_T > 1.2\,\mathrm{GeV}$ (to select an hard process). After all these cuts a remaining contamination ($11.0\pm1.0\%$) of proton dissociative events is still present in the selected sample, it was removed statistically using a Monte Carlo simulation. The acceptance corrections and resolutions effects were determined using dedicated Monte Carlo GRAPE generator [12]. This program is an event generator for dilepton production in *ep* collisions. It is based on exact matrix elements. The program is interfaced to PYTHIA [13] to generate a complete final state. The simulation included both elastic and proton-dissociative events. All generated events were passed through a detector simulation based on GEANT 3.13 [14].

3 Results and discussion

The measured $k_T, W, t, M_{\mu\mu}$ distributions are presented in Fig. 3. The data are compared with a GRAPE Monte Carlo simulation which takes into account elastic and proton dissociative events. The Monte Carlo is normalized to the data. Good agreement is shown between data and simulation.

The differential cross section $d\sigma/du$ was measured, in the aforementioned kinematic region, using the following formula:

$$\frac{d\sigma}{du} = \frac{N \cdot (1 - f_{p\_diss})}{L \cdot A \cdot \Delta u} \tag{12}$$

where N is the number of events in the Δu bin, f_{p_diss} the estimated fraction of proton dissociative events, A the acceptance and L the luminostiy. A detailed study of the systematic uncertainties was made: they are dominated by trigger efficiency. This measured cross section is presented in Fig. 4 and compared with the theoretical curve (BFGMS) [2] in the same kinematical range. For this purpose Eq. (6) was adapted to the muon's analysis:

$$\Phi^2_{\mu\mu/\gamma} = \frac{u^2 + (1-u)^2}{M^2_{\mu\mu}\, u\,(1-u) - m^2_\mu} \tag{13}$$

The LCWF was normalized to the data. The shape of calculated electromagnetic component of the real photon light-cone wave function is in good agreement with the experimental result. The measured cross section was also compared to the GRAPE simulation (dashed histogram) normalized to the luminosity (see Fig. 5). The agreement between data and simulation is within the systematic uncertainties.

This measurement provides the first proof that diffractive dissociation of particles can be reliably used to measure their LCWF. Furthermore it gives support for the method used in previous measurements of the pion LCWF [5] and possible future applications [15].

References

[1] S.J. Brodsky, D.S. Hwang, B.Q. Ma and I. Schmidt, Nucl. Phys. **B 593**, 311 (2001).

[2] S. J. Brodsky, L. Frankfurt, J. F. Gunion, A. H. Mueller and M. Strikman, Phys. Rev. **D50**, 3134 (1994).

[3] I. I. Balitsky et al., Nucl. Phys. **B312**, 509 (1989).

[4] G. Sterman and P. Stoler, Ann. Rev. Nucl. Part. Sci. **43**, 193 (1997).

[5] E791 Coll., E.M.Aitala et al., Phys. Rev. Lett. **86**, 4768 (2001);
E791 Coll., E.M.Aitala et al., Phys. Rev. Lett. **86**, 4773 (2001).

[6] S.J. Brodsky and G.F. Farrar, Phys. Rev. Lett. **31**, 1153 (1973).

[7] ZEUS Coll., U. Holm (ed.), *The ZEUS Detector*. Status Report (unpublished), DESY (1993), available on `http://www-zeus.desy.de/bluebook/bluebook.html`.

[8] G. Abbiendi et al., Nucl. Inst. Meth. **A 333**, 342 (1993).

[9] N. Harnew et al., Nucl. Inst. Meth. **A 279**, 290 (1989);
B. Foster et al., Nucl. Phys. Proc. Suppl. **B 32**, 181 (1993);
B. Foster et al., Nucl. Inst. Meth. **A 338**, 254 (1994).

[10] M. Derrick et al., Nucl. Inst. Meth. **A 309**, 77 (1991);
A. Andresen et al., Nucl. Inst. Meth. **A 309**, 101 (1991);
A. Caldwell et al., Nucl. Inst. Meth. **A 321**, 356 (1992);
A. Bernstein et al., Nucl. Inst. Meth. **A 336**, 23 (1993).

[11] ZEUS Coll., FPC group, A. Bamberger et al., Nucl. Inst. Meth. **A 450**, 235 (2000).

[12] T. Abe et al., *Proc. Workshop on Monte Carlo Generators for HERA Physics*, T.A. Doyle et al. (ed.), p. 566. DESY, Hamburg, Germany (1999). Also in preprint DESY-PROC-1999-02, available on `http://www.desy.de/~heramc/`.

[13] H.-U. Bengtsoon and T. Sjöstrand, Comp. Phys. Comm. **46**, 43 (1987);
T. Sjöstrand, Comp. Phys. Comm. **82**, 74 (1994).

[14] GEANT 3.13: R. Brun et al., CERN DD/EE/84-1 (1987).

[15] D. Ashery, Comments on Modern Physics **2A**, 235 (2002).

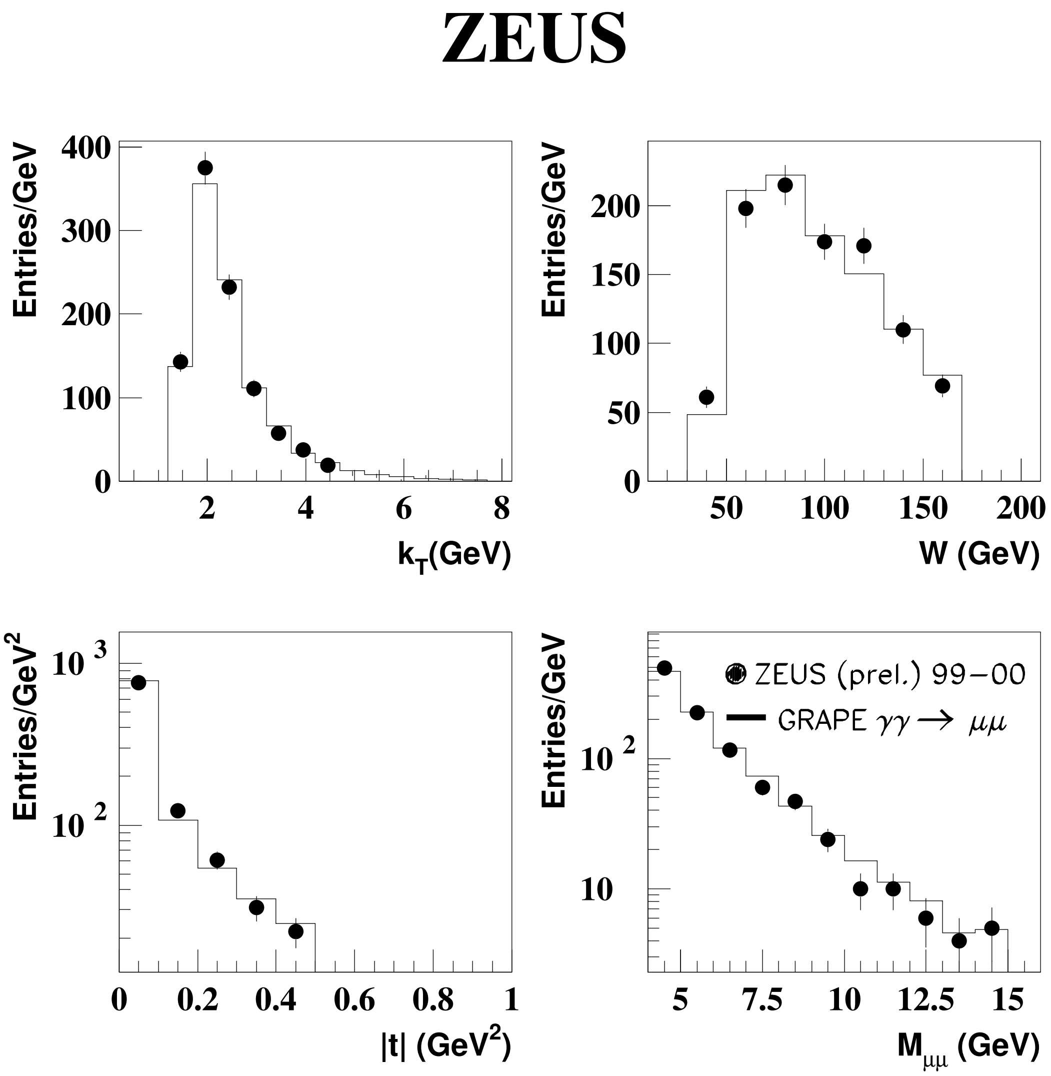

Figure 3: *Number of events reconstructed in the kinematic region* $4 < M_{\mu\mu} < 15$ *GeV,* $30 < W < 170\,GeV$, $|t| < 0.5\,(GeV/c)^2$ *and* $k_T > 1.2$ *GeV/c plotted against* k_T, W, $|t|$ *and* $M_{\mu\mu}$*. The data distributions are shown as the points with statistical errors only. The solid lines show the prediction of the GRAPE generator summing elastic and proton-diffractive components.*

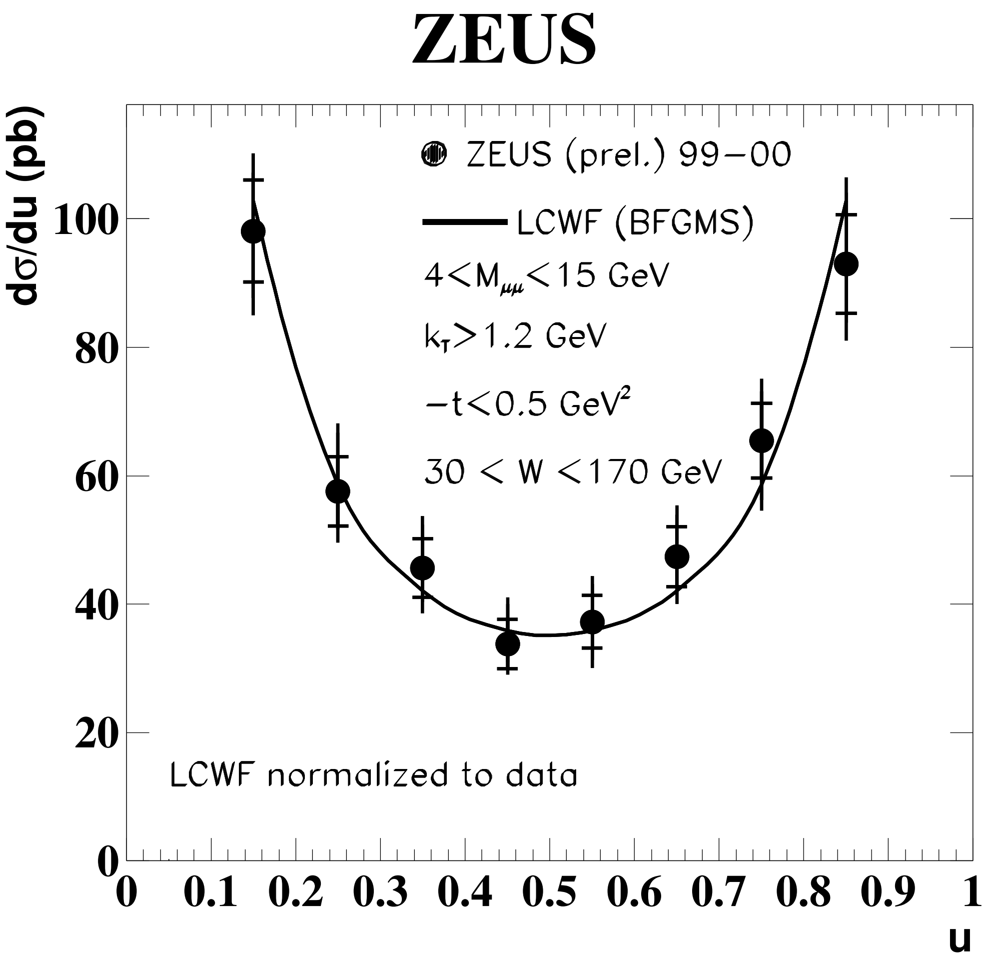

Figure 4: *Differential cross section $d\sigma/du$ measured for $30 < W < 170$ GeV $4 < M_{\mu\mu} < 15$ GeV, $k_T > 1.2$ GeV/c and $-t < 0.5$ $(\mathrm{GeV}/c)^2$. The inner error bars show the statistical uncertainty; the outer error bars show the statistical and systematics added in quadrature. The data points are compared to the prediction of LCWF theory [2]. The theory is normalized to data.*

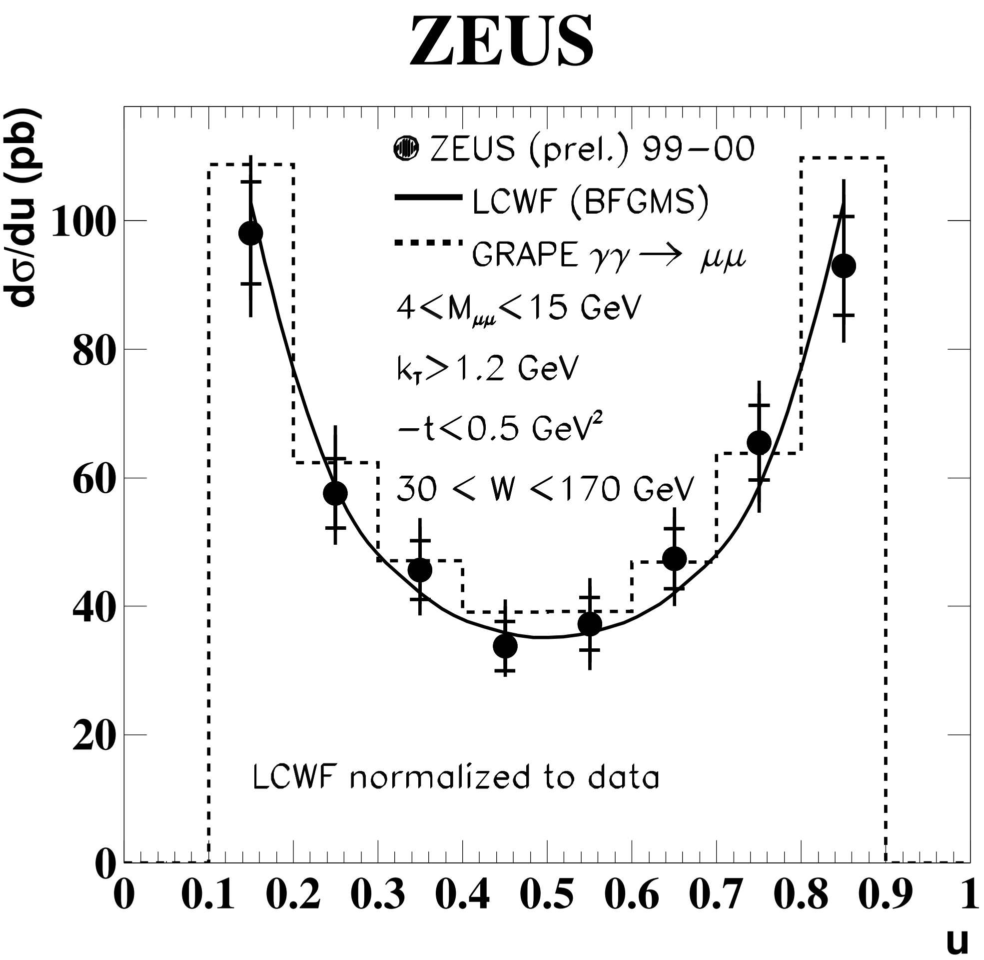

Figure 5: *Differential cross section $d\sigma/du$ measured for $30 < W < 170$ GeV $4 < M_{\mu\mu} < 15$ GeV, $k_T > 1.2$ GeV/c and $-t < 0.5$ (GeV/c)^2. The dashed histogram represents GRAPE simulation normalized to the luminosity. The inner error bars show the statistical uncertainty; the outer error bars show the statistical and systematics added in quadrature. The data points are compared to the prediction of LCWF theory [2] normalized to the data.*